ACS Sustainable Chemistry & Engineering

Research Article

pubs.acs.org/journal/ascecg

Hydrogen Production via Glycerol Steam Reforming over Ni/Al_2O_3: Influence of Nickel Precursors

Gaowei Wu, Chengxi Zhang, Shuirong Li, Zhiping Han, Tuo Wang, Xinbin Ma, and Jinlong Gong*

Key Laboratory for Green Chemical Technology of Ministry of Education, School of Chemical Engineering and Technology, Tianjin University, Tianjin 300072, China

Tianjin Co-Innovation Center of Chemical Science and Engineering, Tianjin 300072, China

Supporting Information

ABSTRACT: This paper describes an investigation regarding the influence of Ni precursors on catalytic performances of Ni/Al_2O_3 catalysts in glycerol steam reforming. A series of Ni/Al_2O_3 is synthesized using four different precursors, nickel nitrate, nickel chloride, nickel acetate, and nickel acetylacetonate. Characterization results based on N_2 adsorption–desorption, X-ray diffraction, H_2 temperature-programmed reduction, H_2 chemisorption, transmission electron microscopy, and thermogravimetric analysis show that reduction degrees of nickel, nickel dispersion, and particle sizes of Ni/Al_2O_3 catalysts are closely dependent on the anion size and nature of the nickel precursors. Ni/Al_2O_3 prepared by nickel acetate possesses the moderate Ni reduction degree, high Ni dispersion, and small nickel particle size, which possesses the highest H_2 yield. Reaction parameters are also examined, and 550 °C and a steam-to-carbon ratio of 3 are optimized. Moreover, coke deposition, mainly graphite species, leads to the deactivation of Ni/Al_2O_3 catalysts in glycerol steam reforming. Nickel chloride-derived Ni/Al_2O_3 catalysts suffer from severe coke deposition and low reaction activity due to large Ni particle size, low Ni dispersion, and residual chloride.

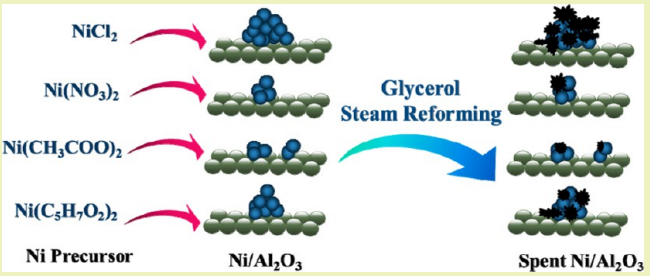

KEYWORDS: *Nickel precursor, Ni/Al_2O_3, Glycerol steam reforming, Hydrogen production, Coke deposition*

INTRODUCTION

Hydrogen has wide applications in the chemical and petroleum industries and is also identified as a promising clean energy vector for fuel cell devices.[1,2] Because of the intrinsic drawbacks of fossil fuels including the limited sources and environmental concerns, the global demand for renewable energy including hydrogen rapidly grows. Nowadays, H_2 is mainly produced from steam reforming of natural gas in industry, but this process does not contribute to the reduction of greenhouse gases and the sustainable development of the global economy.[3−5] Therefore, the production of hydrogen from renewable sources especially from biomass attracts increased interest considering the environmental impact.[3,6−9] Among various bioderived feedstocks, glycerol is promising because of its relatively high hydrogen content, nontoxicity, and ease to store and handle.[10] Notably, approximately 10 wt% glycerol is produced as a byproduct in converting triglycerides into biodiesel.[11−14] Glycerol can also be produced by fermentation of sugars or as a byproduct of the industrial conversion of lignocellulose into ethanol.[12] With rapid growth in the production of biodiesel and bioethanol, glycerol on the global market is anticipated to be redundant.[14] This makes conversion of bioderived glycerol to valuable chemicals and hydrogen not merely environmentally friendly but also potentially economical.

Glycerol steam reforming (GSR) is an endothermic process and is usually operated at high temperature (e.g., above 400 °C), yet the combination of this process with other exothermic ones (e.g., Fischer–Tropsch, methanol syntheses) contributes to an available energy-efficient route for H_2 production.[12] Additionally, GSR can be operated at ambient pressure favoring high selectivity to H_2 compared to aqueous phase reforming.[15,16]

Ideally, GSR takes place according to the following stoichiometric equation

$$C_3H_8O_3 + 3H_2O \leftrightarrow 7H_2 + 3CO_2\ \Delta H_{298\,K} = +128\ \text{kj/mol} \quad (1)$$

However, the reaction pathway is quite complex, and primary reactions in GSR include glycerol decomposition (eq 2), water gas shift reaction (WGSR, eq 3), and steam reforming (SR) of methane (eq 4).[5,17]

$$C_3H_8O_3 \leftrightarrow 4H_2 + 3CO\ \Delta H_{298\,K} = +250\ \text{kJ/mol} \quad (2)$$

$$CO + H_2O \leftrightarrow CO_2 + H_2\ \Delta H_{298\,K} = -41\ \text{kJ/mol} \quad (3)$$

Received: April 26, 2013
Revised: May 26, 2013
Published: May 30, 2013

dx.doi.org/10.1021/sc400123f | ACS Sustainable Chem. Eng. 2013, 1, 1052−1062

$$CH_4 + 2H_2O \leftrightarrow CO_2 + 4H_2 \ \Delta H_{298\,K} = +165\ kJ/mol \quad (4)$$

Catalysts utilized in GSR primarily include Ni,[11,18] Co,[4] Pt,[19] Ru,[20] Rh,[17] and Ir,[21] which have been extensively discussed in previous work[22,23]. Bimetallic catalysts are also widely employed in GSR[24] due to the ensemble and/or ligand effects. Among these active metals, Ni has been widely investigated due to its known activity in cleavage of C−C, O−H, and C−H bonds and WGSR.[21,25−29] Lower cost and higher availability of Ni compared to noble metals also make it widely applied in the preparation of SR catalysts.[30,31]

Nickel-based catalysts are commonly prepared by impregnating a nickel precursor, followed by drying and thermal treatments. As reported in previous studies, the nature of nickel precursors used in the catalyst preparation process is an indispensable parameter affecting catalytic performance.[32−39] Alumina is the most widely used support material for commercial Ni catalysts. Notable features of alumina supports are their ability to highly disperse the active metal phase and good mechanical properties.[40]

It has been well established that the type of nickel species leads to the different interaction with γ-Al_2O_3 and thus shows different reduction behavior.[41] Xie et al.[42] showed that the dispersion capacity of NiO was in well accordance with its precursor, and the larger size of nickel acetate resulted in lower dispersion capacity of its derived NiO on γ-Al_2O_3 in comparison with nickel nitrate-derived NiO. Lu et al.[36] investigated the effect of nickel precursor in CO_2 reforming of methane and demonstrated that Ni/Al_2O_3 based on nickel nitrate exhibited higher catalytic activity and stability than the other two catalysts derived from nickel chloride and nickel acetylacetonate. Additionally, carbon deposition on Ni catalysts derived from inorganic precursors was more severe than that on the organic precursor-derived catalysts. Furthermore, a Ni/Al_2O_3 catalyst prepared using a nickel chloride precursor contained relatively large nickel particles upon reduction and showed a lower initial conversion than the nickel nitrate-derived catalyst for hydrodechlorination of 1,1,2-trichloroethane.[33] Yet, Fan et al.[38] pointed out that the catalytic activity of the nickel acetate-derived Ni/Al_2O_3 catalyst was much higher than that of the nickel nitrate-derived catalyst for hydrogenation of α-pinene, and the different hydrogenation activity of Ni/Al_2O_3 was correlated to the different ratio of Ni^{2+} ions in the tetrahedral and octahedral sites of γ-Al_2O_3 and the different reduction degree of the NiO/Al_2O_3 precursors.

This paper describes our understanding of the influence of nickel precursors on the catalytic properties of Ni/Al_2O_3 in GSR. A series of Ni/Al_2O_3 catalysts were prepared by impregnating nickel nitrate, nickel chloride, nickel acetate, and nickel acetylacetonate and were characterized by various characterization techniques including N_2 adsorption−desorption, X-ray diffraction (XRD), H_2 temperature-programmed reduction (H_2-TPR), H_2 chemisorption, NH_3 temperature-programmed desorption (NH_3-TPD), X-ray photoelectron spectra (XPS), transmission electron microscopy (TEM), and thermogravimetric analysis (TGA). The catalytic activity of the catalysts was investigated in GSR at a temperature of 450−650 °C and a steam-to-carbon (S/C) ratio in a range of 1−5. Stability tests of 30 h were also carried out to examine the origin of the deactivation of the Ni/Al_2O_3 catalysts.

EXPERIMENTAL SECTION

Catalysts Preparation. Ni/Al_2O_3 catalysts with 15 wt% Ni loading were prepared by a wetness impregnation method. Four kind of Ni precursors with different anion sizes were used in this work including nickel nitrate, nickel chloride (98.0%, Tianjin Guangfu Fine Chemical Institute), nickel acetate (98.0%, Tianjin Damao Chemical Co., Ltd.), and nickel acetylacetonate (98%, J&K Scientific Ltd.). Commercial γ-Al_2O_3 was pretreated in a muffle furnace at 700 °C for 4 h and then impregnated in ethanol solution of each aforementioned nickel precursor by mechanical agitation at 60 °C for 12 h. Then the solution was evaporated at 60 °C using a vacuum rotary evaporator until the ethanol was removed. The resultant solids were dried at 120 °C for 12 h and then calcined at 700 °C for 4 h. The catalysts synthesized by nickel nitrate, nickel chloride, nickel acetate, and nickel acetylacetonate are labeled as Ni−N, Ni−C, Ni−AC, and Ni−AA, respectively.

Catalyst Characterization. XRD measurements were performed with 2θ values between 10 and 85° by using a Rigaku C/max-2500 diffractometer employing the graphite filtered Cu Kα radiation (λ = 1.5406 Å). The Scherrer equation was used to estimate the mean Ni crystallite size based on the diffraction peaks of the Ni (200) facet.

Textual properties of the catalysts were measured with a Micromeritics Tristar 3000 analyzer by nitrogen adsorption at −196 °C. The samples were degassed at 300 °C for 4 h before measurements. This instrument employed the BET method by measuring the quantity of nitrogen absorbed at −196 °C, and the cumulative volumes of pores were obtained by the BJH method from the desorption branches of the adsorption isotherms.

H_2-TPR was employed to analyze the reduction behavior of the catalysts by using a Micromeritics AutoChem 2920 apparatus. A powered sample (50 mg) was pretreated at 400 °C for 1 h under flowing Ar (30 mL min^{-1}). Upon cooling to 50 °C, a flow rate of 30 mL min^{-1} of 10 vol% H_2/Ar was used for the reduction, and the temperature was increased linearly from 50 to 1000 °C at 10 °C min^{-1}.

Dispersion of nickel was studied employing H_2 chemisorption. For each run, 200 mg of catalyst were prereduced with 10 vol% H_2/Ar at 700 °C for 1 h and then flushed with Ar at 700 °C for 30 min. H_2 chemisorption was carried out at 50 °C by injection pulses of 10 vol% H_2/Ar (0.5082 mL) every 4 min until the consumption peaks became stable (about 10 pulses).

NH_3-TPD was conducted on a Micromeritics AutoChem 2920 apparatus. A powered sample (200 mg) was first prereduced with 10 vol% H_2/Ar at 700 °C for 1 h and then flushed with Ar at 700 °C for 30 min. Upon cooling to 100 °C, the sample was saturated with NH_3 by flowing 10 vol% NH_3/N_2 at 100 °C for 30 min and then flushed with pure helium (30 mL min^{-1}) for 1 h before desorption analysis. NH_3-TPD analysis was carried out with a ramp of 10 °C min^{-1} from 100 to 1000 °C in a He flow of 30 mL min^{-1}.

XPS was operated in a Perkin−Elmer PHI 1600 ESCA system with Mg Kα 1253.6 eV radiation as the excitation source. The sample was mounted on the specimen holder by means of double-sided adhesive tape. Spectra were collected in steps of 0.15 eV.

TEM was conducted to characterize the morphology of catalysts employing a JEM-2100F transmission electron microscope at 200 kV. The sample was first dispersed in ethanol and supported on lacey-Formvar carbon on a 200 mesh Cu grid before TEM images were recorded.

TGA (STA449F3 NETZSCH Corp.) was used to investigate the carbon deposition of spent catalysts. The sample was heated from room temperature to 750 °C at the rate of 10 °C min^{-1} in air (100 mL min^{-1}).

Thermodynamic Calculation and Catalytic Tests. The thermodynamics of the GSR was analyzed by using the HSC Chemistry software. H_2, CO, CO_2, CH_4, H_2O, and unreacted glycerol were considered as the possible components, and the equilibrium composition of the reaction is calculated as a function of the reaction temperature and the S/C ratio.[27,43]

Catalytic tests were carried out at atmospheric pressure in a quartz fixed-bed reactor loaded with 150 mg catalyst (20−40 mesh) mixed

with 1 mL quartz particles. Before the test, the catalysts were reduced at 700 °C in situ for 1 h in a flow of 10 vol% H_2/N_2. The liquid solution with a certain S/C ratio was fed through an HPLC pump into a heated chamber (250 °C) to evaporate the solution completely in the stream of N_2 before reaction. The products were first condensed through a cooler, and the incondensable gas species were analyzed online by two gas chromatographs. One is equipped with a flame ionization detector (FID) and a Porapak-Q column with N_2 as a carrier gas to analyze the organic species such as methane, ethylene, and ethane. The other one is integrated with a thermal conductivity detector (TCD) and a TDX-01 column using He as a carrier gas to monitor hydrogen, carbon dioxide, carbon monoxide, and methane. Products in the condensed liquid phase were analyzed on an Agilent 7890A gas chromatographs equipped with a DB-Wax GC column.

The performance of the catalyst is presented in terms of H_2 mol yield and C-containing gas products selectivities (eq 5).

$$\%\text{Selectivity of } i = \frac{i \text{ mol}}{(\sum i \text{ species}) \text{ mol produced}} \times 100 \quad (5)$$

where i represents CO, CO_2, CH_4, C_2H_4, and C_2H_6.

RESULTS

Characterization of Fresh Catalysts. Diffraction patterns of reduced Ni/Al_2O_3 catalysts are shown in Figure 1. The

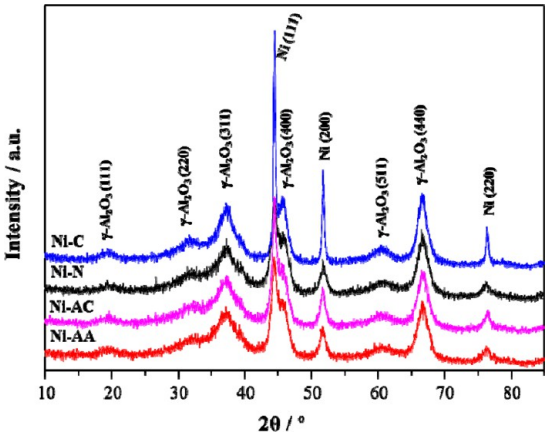

Figure 1. XRD profiles for Ni/Al_2O_3 catalysts upon reduction at 700 °C.

diffractograms of all four reduced catalysts show reflections at 19.5°, 31.9°, 37.6°, 45.9°, 60.9°, and 67.0°. These reflections are assigned to γ-Al_2O_3 with low crystallinity.[44] Characteristic peaks of Ni ($2\theta^\circ \approx 44.6^\circ$, 51.3°, and 76.1°) were also detected in all catalysts. Noticeably, the reflections of $NiAl_2O_4$ spinel ($2\theta^\circ \approx$ 19.0°, 31.3°, 36.9°, 44.8°, 59.4°, and 65.2°) are very close to those of γ-Al_2O_3, and it is difficult to confirm the existence of $NiAl_2O_4$ in synthesized samples by means of XRD. Yet, the relative intensity of the main diffraction peaks can also be used as a criterion for the presence of phases in the catalysts.[45,46] According to JCPDS 10-0425 and JCPDS 21-1152, the ratios of peak intensity at about 37° and 45° for γ-Al_2O_3 and $NiAl_2O_4$ are 80/100 and 100/65, respectively. The ratios for the corresponding peaks in Figure 1 range from 0.82 to 0.91, higher than that of γ-Al_2O_3. Hence, we could confirm the presence of $NiAl_2O_4$ in the reduced catalysts. Additionally, nickel peaks on Ni−C are sharper compared to other catalysts, indicating larger nickel particle size and lower nickel dispersion.[36]

Quantitative calculations of nickel crystallite diameter based on Ni (200) reflection and the Scherrer equation are shown in Table 1. Nickel particle size follows an order of Ni−AC < Ni−N < Ni−AA < Ni−C. However, the average pore diameter and pore volume of the four catalysts (Table 1) differ slightly, which are all lower than the Al_2O_3 support. BET surface areas of the prepared catalysts also present obvious decrease compared to the support. This phenomenon could be caused by the pore-blocking during impregnating the precursors.

Table 1. Characteristics of Ni/Al_2O_3 Catalysts

sample	BET surface area ($m^2\ g^{-1}$)	average pore diameter (nm)	pore volume ($cm^3\ g^{-1}$)	Ni crystal size of fresh and spent catalysts (nm)[a]
Al_2O_3	192	10.0	0.56	/
Ni−AC	158	9.8	0.47	9.4/9.5
Ni−AA	154	10.0	0.48	12.5/12.6
Ni−N	149	10.2	0.44	9.8/9.5
Ni−C	133	10.9	0.47	15.7/17.3

[a]Determined by the Sherrer equation from Ni (200) plane of XRD patterns.

H_2-TPR was used to study the reducibility and the type of Ni species in Ni/Al_2O_3 catalysts (Figure 2). The original TPR profiles first subtracted the background and then were fit into three peaks using Gaussian-type functions. The corresponding area percentages of the fitted peaks are summarized in Table 2.

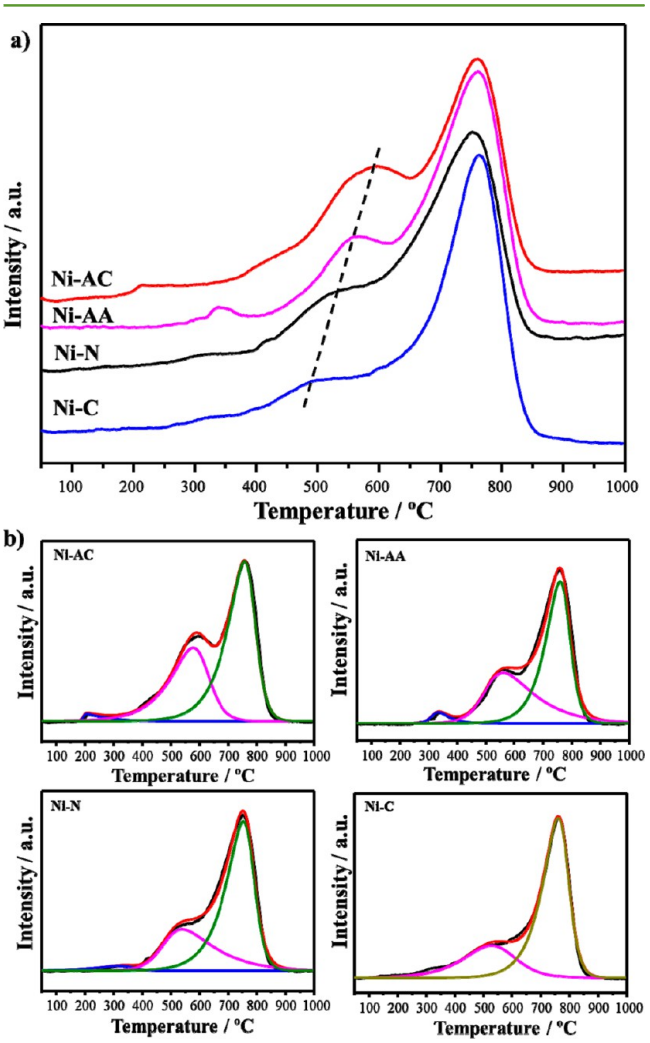

Figure 2. TPR profiles of Ni/Al_2O_3 catalysts: (a) original profiles and (b) fitted profiles.

dx.doi.org/10.1021/sc400123f | ACS Sustainable Chem. Eng. 2013, 1, 1052−1062

Table 2. Properties Obtained from TPR Profiles and H_2 Chemisorption

	area percentage (%)[a]				
sample	peak 1	peak 2	peak 3	metal dispersion (m^2 g_{cat})[b]	nickel reduction degree (%)[c]
Ni−AC	1.9	37.7	60.4	0.88	61.2
Ni−AA	3.2	41.1	55.7	0.31	93.6
Ni−N	3.1	32.7	64.3	0.72	65.9
Ni−C	0	28.3	71.7	0.08	49.8

[a]Peaks 1, 2, and 3 correspond to the peaks at low, medium, and high temperatures, respectively. [b]Determined from H_2 chemisorption. [c]Determined from the amount of H_2 consumed (calculated from the reduction peak area) in TPR divided by that consumed in reduction conditions (700 °C for 1 h).

An intense H_2 consumption peak around 750 °C and a shoulder peak at 550 °C can be observed, which are respectively attributed to the reduction of Ni^{2+} ions incorporated into tetrahedral and octahedral vacancies, two kinds of surface vacant sites on the preferentially exposed (110) plane of γ-Al_2O_3.[38,41,47,48] Relative quantities of the two peaks can be obtained based on the peak areas of different nickel species in each sample. Ni−C indicates the strongest peak and largest area percentage at 750 °C, proving the existence of the highest fraction of tetrahedral Ni^{2+} species among Ni/Al_2O_3 catalysts. Correspondingly, the amount of octahedral Ni^{2+} species in Ni−C is the least among the four samples, whereas more octahedral Ni^{2+} species is present in Ni−AA than the others. Additionally, the dashed line in Figure 2 indicates the reduction temperatures of the shoulder peaks increase gradually from Ni−C to Ni−AC. Specifically, the shoulder peak of Ni−AC presents the highest reduction temperature. Furthermore, the reduction peaks occurring between 200 and 400 °C correspond to the reduction of NiO.[49,50] From Figure 2, a distinct reduction peak could be observed at 350 °C in the curve of Ni−AA catalyst, which also corresponds to the 3.2% of all Ni species.

Ni/Al_2O_3 catalysts prepared by different nickel precursors possess distinct metal dispersion (Table 2). Ni−AC has the highest nickel dispersion, followed by Ni−N, Ni−AA, and Ni−Cl. This order is opposite to that of Ni crystal size. We need to mention that residual chloride on the Ni−C was detected by XPS (Figure S1, Supporting Information). The presence of residual chloride has negative effect on hydrogen chemisorption, and this leads to a low metal dispersion.[51] Ni−AA presents the highest reduction degree (93.6%). It should be noted that all the reduction degree was less than 100% due to the existing of $NiAl_2O_4$ in reduced samples.

The morphology of Ni/Al_2O_3 catalysts synthesized from different precursors is presented in Figure 3, together with the particle size distribution. It is clear that the metal particles are uniformly dispersed over alumina and distributed within a narrow size range for the Ni−AC and Ni−N catalysts. However, Ni−C has larger Ni particle size and wider distribution range than those of Ni−AA; these results are consistent with XRD data.

Catalytic Performances in Glycerol Steam Reforming. *Effect of Reaction Temperature.* The activity of Ni/Al_2O_3 catalysts in the GSR performed from 450 to 650 °C at the stoichiometric S/C ratio is measured at steady state of reaction and the obtained results are illustrated in Figure 4. A full conversion of glycerol was observed under test conditions on

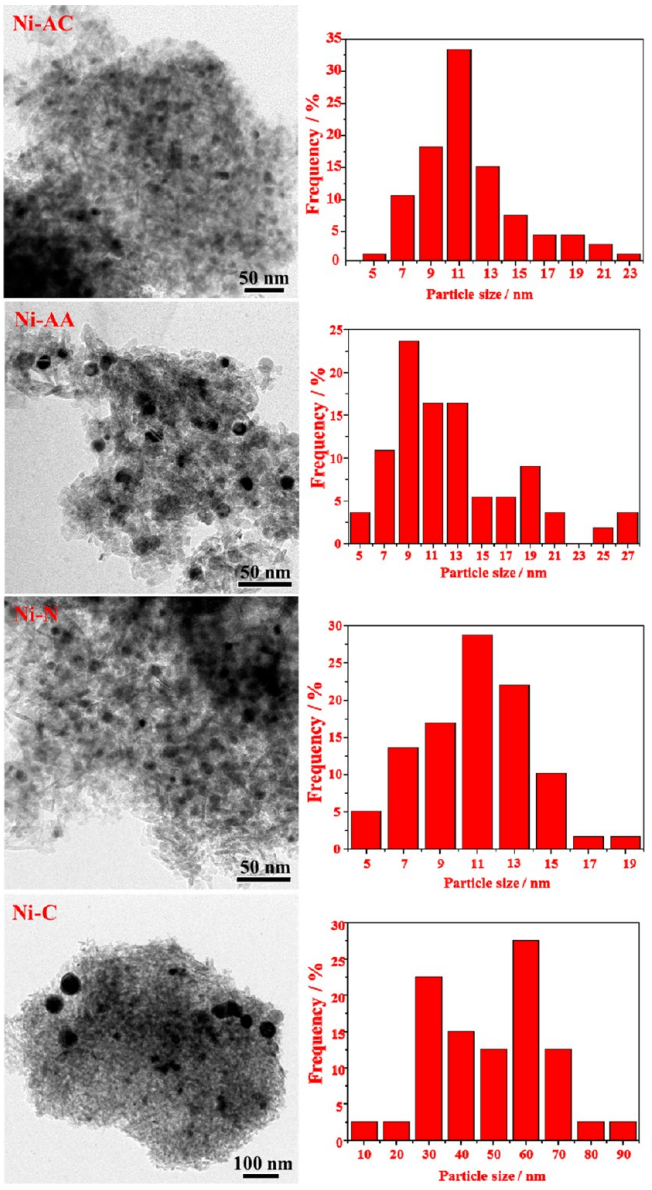

Figure 3. TEM images of reduced Ni/Al_2O_3 catalysts and particle size distribution.

all the samples. Indeed, thermodynamic analysis proves that glycerol can be completely converted at the temperature region. Shen et al.[21] also observed the complete conversion of glycerol at 450 °C for Ni/CeO_2. Similar distribution of condensable products were observed for the four catalysts at the same reaction condition, and the main products were trace amounts of acetaldehyde, methanol, ethanol, propanal, acetone, allyl alcohol, 1-hydroxy-2-propanone, and 1,2-propandiol. This result suggests that the reaction pathway of GSR over nickel-based catalysts could be similar, which has also been proposed in previous work.[52,53] Therefore, only hydrogen molar yield and selectivities of C-containing gas-phase products were presented to compare the activity of difference Ni/Al_2O_3 catalysts.[5,19,27]

For all four catalysts, H_2 yield increases with increasing the reaction temperature from 450 to 550 °C due to the endothermic nature of GSR, and the differences were most pronounced from 550 to 650 °C. H_2 yield of Ni−AC and Ni−N catalysts then remains constant up to 650 °C, and the tendency can be explained by the thermodynamic equilibrium,

dx.doi.org/10.1021/sc400123f | ACS Sustainable Chem. Eng. 2013, 1, 1052−1062

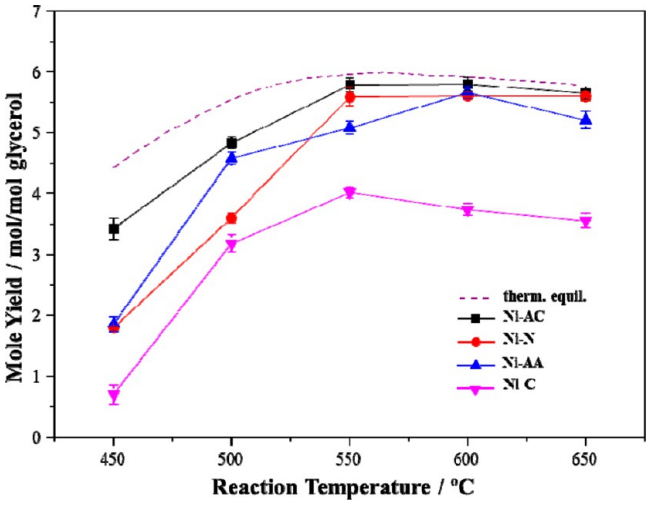

Figure 4. Effect of reaction temperature on H_2 molar yield of Ni/Al_2O_3 catalysts. Reaction condition: S/C = 3, WHSV = 6.6 h^{-1}, and atmospheric pressure.

which is also in agreement with previous results.[25,27] It still rises obviously for Ni−AA catalyst from 550 to 600 °C and then decreases from 600 to 650 °C, whereas Ni−C presents a decreasing trend above 550 °C. It should be mentioned that Ni−AC possesses the highest activity, and the hydrogen yield is close to the thermodynamic equilibrium over the whole investigated temperature range.

The distribution of C-containing gas-phase products over the four catalysts is shown in Figure 5. From the thermodynamic point of view, WGSR is favored at low temperature and methane SR is favorable at high temperature.[18] Thus, the CO_2/CO ratios decrease gradually as the temperature increases, and the selectivities of CH_4 present the same downward trend in Figure 5. Notably, CO_2/CO ratios over Ni−AC and Ni−N are obviously higher compared to other catalysts at the same reaction condition. Less CH_4 is formed at elevated temperature. Interestingly, significant levels of ethylene and ethane are observed at low reaction temperature. We also note that there are no obvious changes in the CO_2/CO ratios of Ni−C through the whole temperature range; C_2H_4 and C_2H_6 are even present in the reaction products of Ni−C even at 650 °C. The variations of C_2H_4 and C_2H_6 in the products are attributed to Ni capacity to break C−C bonds, which could be enhanced at high temperature.[18]

Effect of S/C Ratio. Upon analyzing the effects of reaction temperature on the catalytic performance of Ni/Al_2O_3, the optimized temperature of 550 °C was selected for further investigation of other experimental parameters (e.g., S/C ratios) considering that the H_2 yield reaches the terrace according to the experimental and thermodynamic results. Additionally, steam reforming is an energy-intensitive process, and low reaction temperature is practically desriable. Glycerol

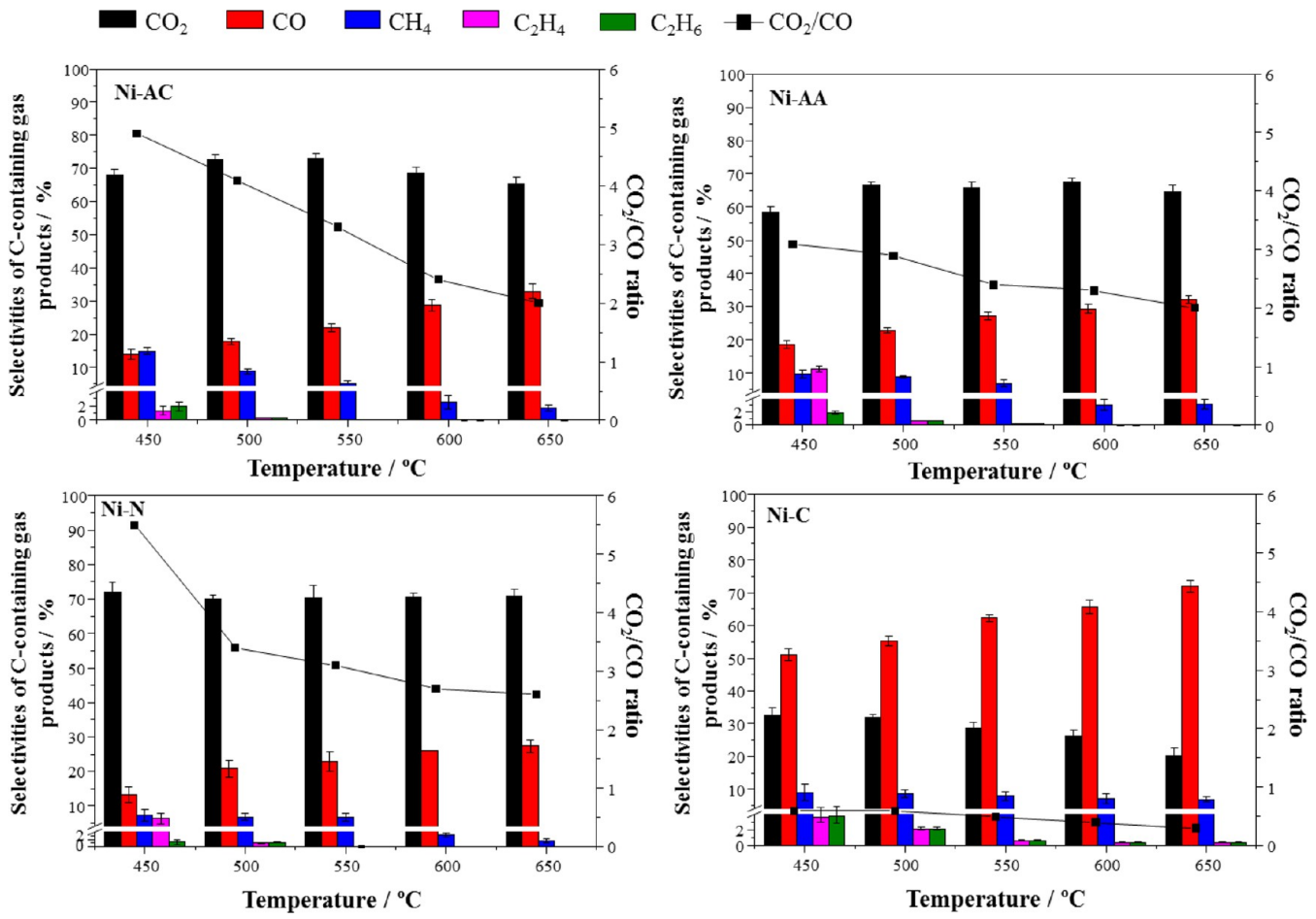

Figure 5. Effect of reaction temperatures on the selectivities (%) of C-containing gas-phase products of Ni/Al_2O_3 catalysts. Reaction condition: S/C = 3, WHSV = 6.6 h^{-1}, and atmospheric pressure.

content in the feed was changed to achieve the target S/C ratio, and the results are depicted in Figure 6. Glycerol is totally converted at the chosen reaction conditions. The increase in S/C ratio from 1 to 3 promotes H_2 yield significantly over all Ni/Al_2O_3 catalysts because the increase in water content in the feed promotes a forward reaction of WGSR, and more H_2 and CO_2 are produced.[53] With a further increase in S/C ratio from 3 to 5, H_2 yield goes up slightly, in agreement with the thermodynamic analysis. The maximum H_2 yield was found to be 6.2 mol/mol glycerol for Ni–AC under S/C of 5, followed by Ni–N and Ni–AA. The Ni–C catalyst shows the lowest H_2 yield in all S/C ratios investigated.

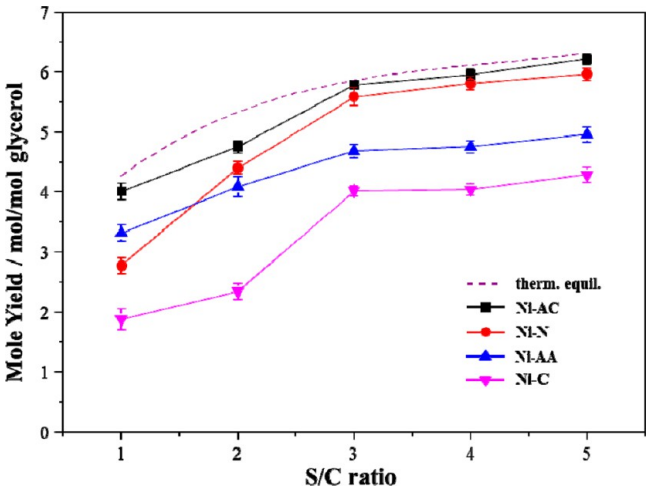

Figure 6. Effect of S/C ratios on H_2 molar yield of Ni/Al_2O_3 catalysts. Reaction condition: reaction temperature = 550 °C, WHSV = 6.6 h^{-1}, and atmospheric pressure.

Figure 7 illustrates the effect of Ni precursor on the selectivities of C-containing gas-phase products under different S/C ratios. With the increase in S/C ratio, CO_2 selectivities of Ni–AC, Ni–AA, and Ni–N catalysts increase gradually, and CO selectivities decrease correspondingly due to the favorable thermodynamic of WGSR. Ni–AC presents higher CO_2/CO ratios than other catalysts through the S/C ratios. However, there are no significant changes in the CO_2 and CO selectivities of the Ni–C sample. CH_4 selectivities of all four catalysts are prone to be less affected by S/C ratios. By contrast, more C_2H_4 and C_2H_6 were observed in the Ni–C than Ni–AA and Ni–N; however, they were not detected from S/C = 2 to 5 for Ni–AC. Consequently, we conclude that 550 °C and S/C = 3 are the optimized reaction parameters considering the efficiency to produce H_2.

Stability Test. The stability of Ni/Al_2O_3 catalysts was tested under atmospheric pressure with reaction temperature = 550 °C and S/C = 3. All glycerol conversions (not shown) are found to be 100%. From Figure 8, a deactivation phenomenon is noticed on all the catalysts; however, the deactivation degree

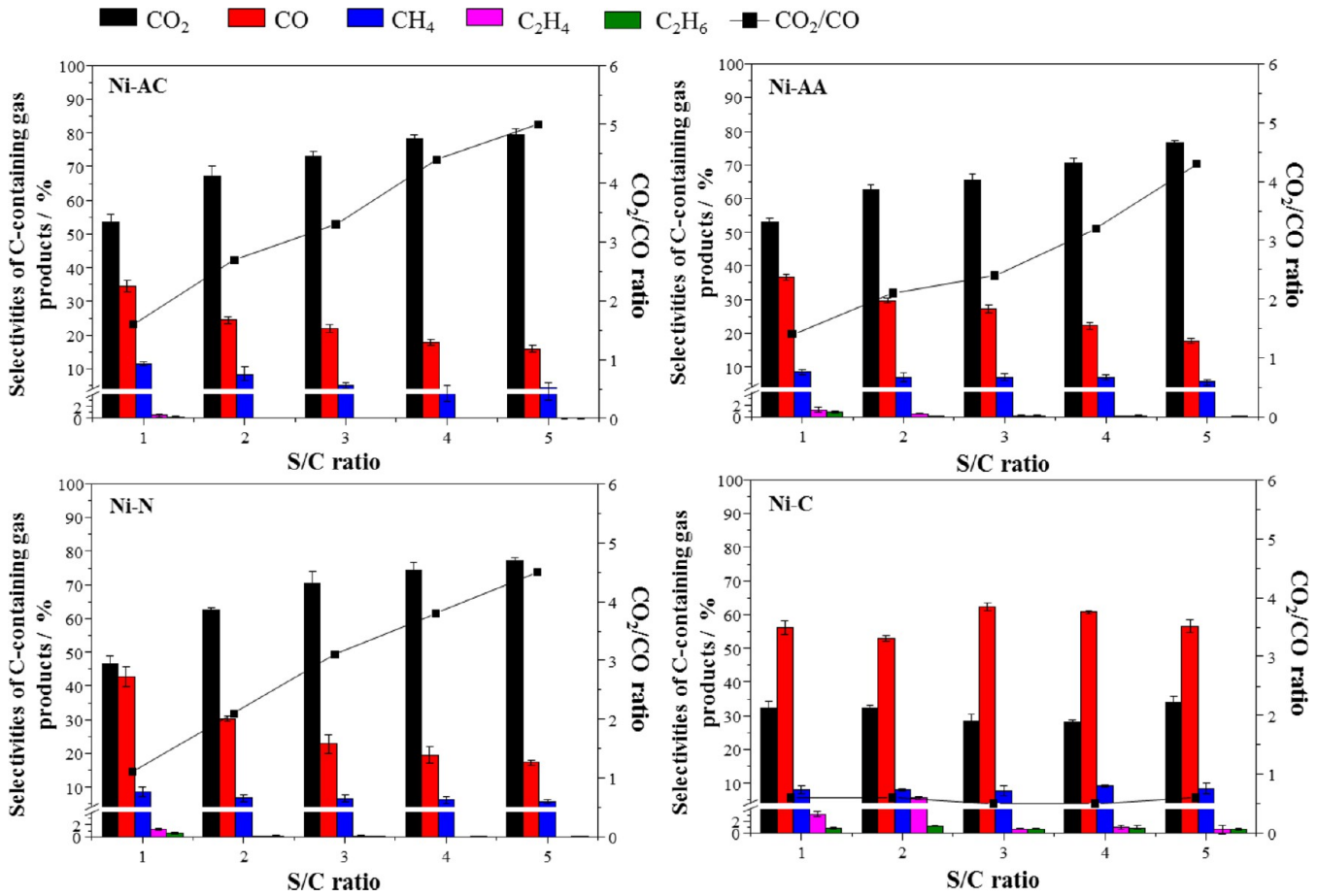

Figure 7. Effect of S/C ratios on the selectivities (%) of C-containing gas-phase products of Ni/Al_2O_3 catalysts. Reaction condition: reaction temperature = 550 °C, WHSV = 6.6 h^{-1}, and atmospheric pressure.

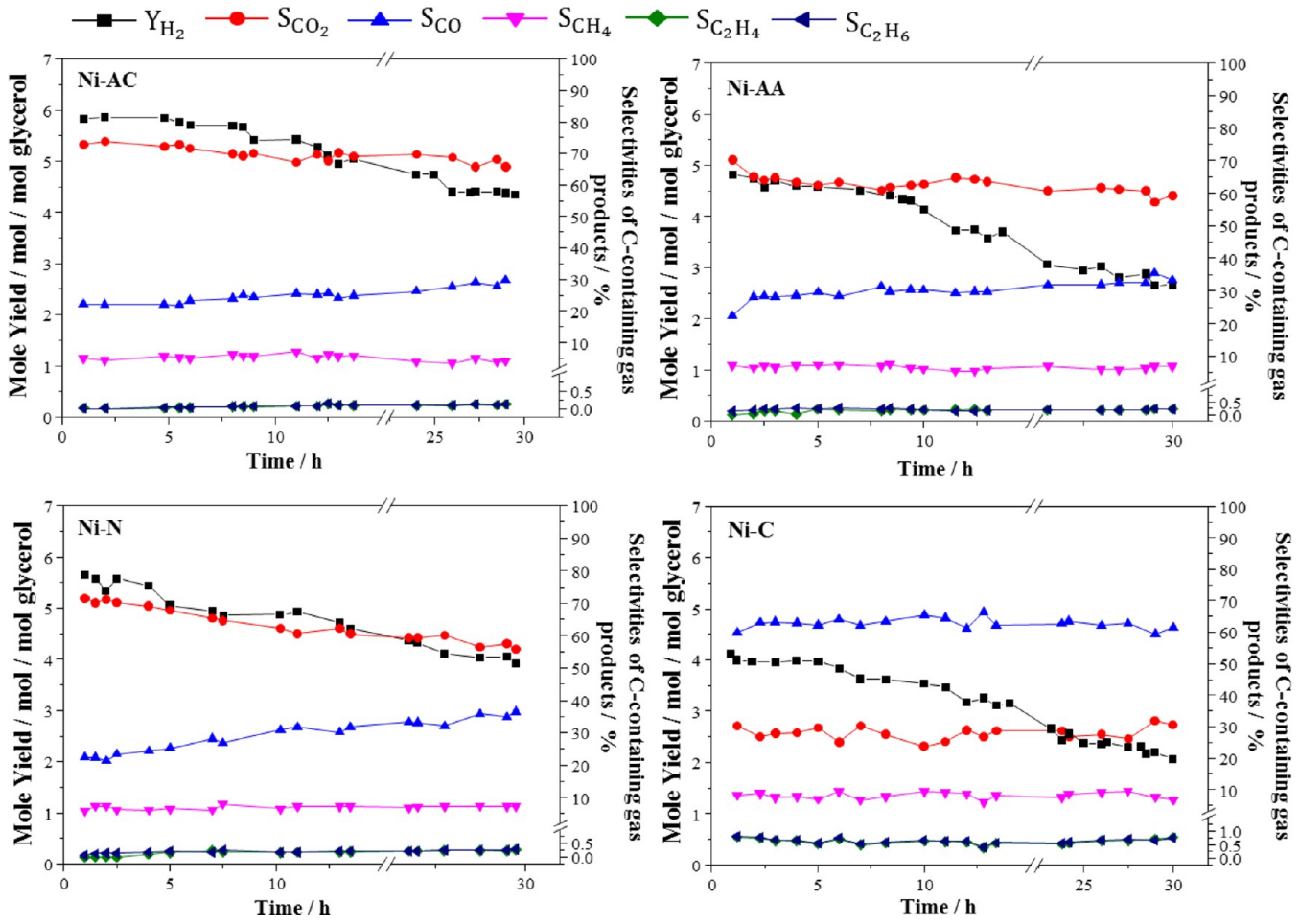

Figure 8. Stability tests of Ni/Al_2O_3 catalysts. Reaction condition: reaction temperature = 550 °C, S/C = 3, WHSV = 6.6 h^{-1}, and atmospheric pressure.

for each catalyst is obviously distinguishing. The highest H_2 yield, together with CO_2 selectivity, is attained over the Ni−AC sample throughout the stability test. Additionally, Ni−N presents higher initial H_2 yield (about 5.6 mol/mol glycerol) than Ni−AA and decreased gradually to 3.9 mol/mol glycerol at the end of the test. Comparatively, the lowest H_2 yield and CO_2 selectivity were yielded using the Ni−C catalyst. A certain amount of C_2H_4 and C_2H_6 (about 0.7 mol %) were also observed in the gas products of Ni−C. CH_4 formation is quite stable in the course of time with all the catalysts.

Characterization of Spent Catalysts. XRD patterns of spent Ni/Al_2O_3 catalysts upon the stability test are presented in Figure 9. Quartz sand mixed with spent catalysts was not completely separated and was also detected in the XRD patterns. The characteristic peaks of Ni and γ-Al_2O_3 phases still exist in all the spent catalysts, and the corresponding Ni particle size of each Ni/Al_2O_3 catalysts (Table 1) stayed almost the same after 30 h reaction.

The amount of carbonaceous species deposited on the spent catalysts and qualitatively the type of these mentioned deposits were determined by TGA results (Figure 10). The mass loss curves present a slight increase from the beginning (at about 300 °C) and then swiftly decline. It can be observed that the mass loss started from 500 °C, and the amount of carbon deposition followed the order Ni−AC < Ni−N < Ni−AA < Ni−C. Carbon deposition accounts for 48.0 wt% of spent Ni−C catalysts.

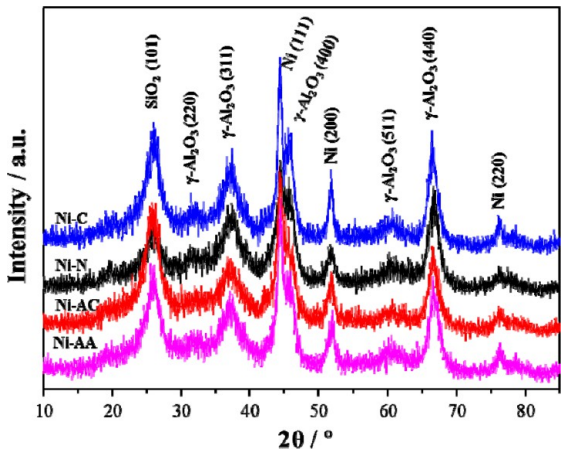

Figure 9. XRD patterns of spent Ni/Al_2O_3 catalysts.

Figure 11 shows the morphology of spent Ni/Al_2O_3 catalysts. Compared with fresh catalysts (Figure 3), it can be revealed that all the catalyst surface appears to be covered by coke deposition to some degree.[17] Filamentous carbon species was also observed in the Ni−C sample. In terms of metal sintering, it should be noted that Ni particles size distribution does not change significantly, in accordance with the fresh catalysts.

dx.doi.org/10.1021/sc400123f | ACS Sustainable Chem. Eng. 2013, 1, 1052−1062

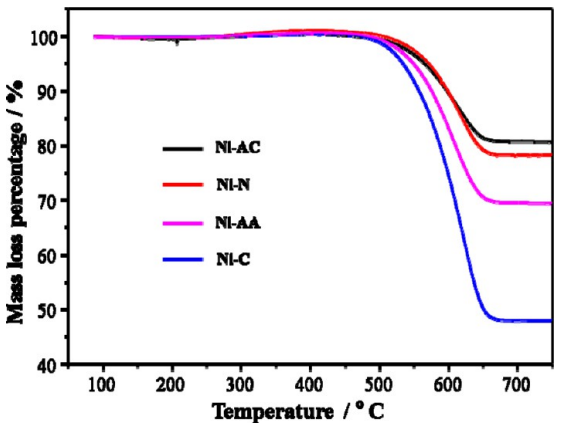

Figure 10. TG profiles for spent Ni/Al_2O_3 catalysts.

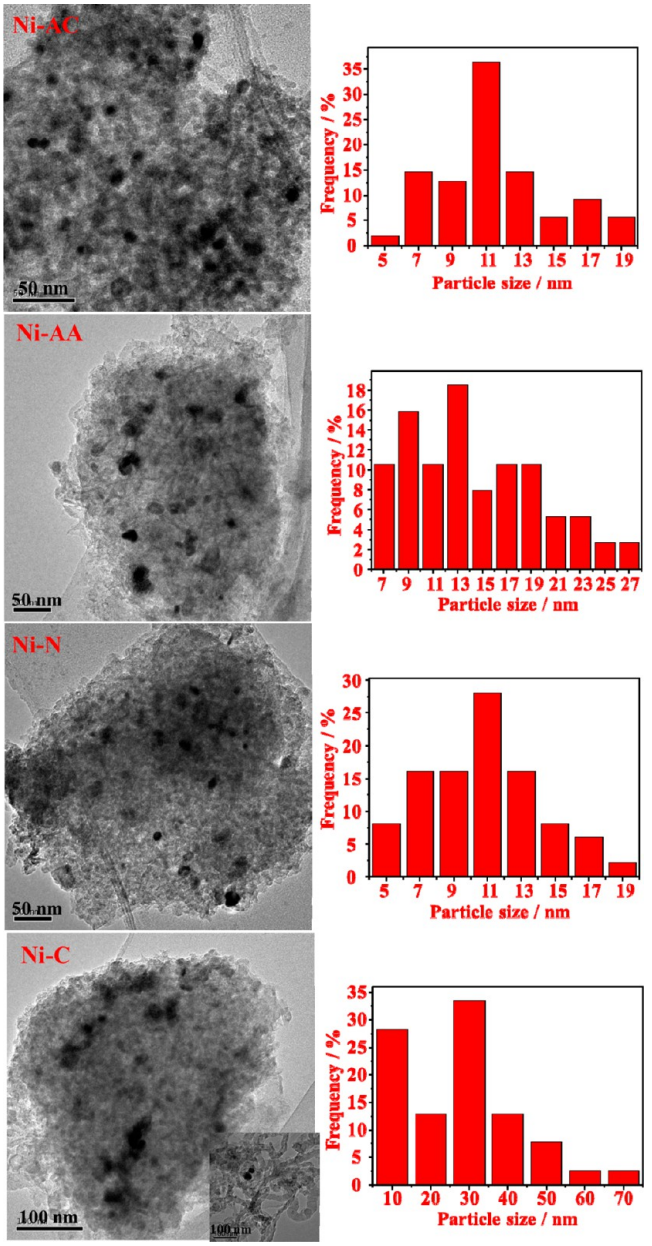

Figure 11. TEM images of spent Ni/Al_2O_3 catalysts and particle size distribution.

DISCUSSION

Ni/Al_2O_3 catalysts prepared based on different nickel precursors have presented distinct characteristics in Ni particle size, dispersion, and reduction degree upon reduction at 700 °C. Because the nickel loading and calcination temperature are kept the same, the relationship between these differences in characteristics and nickel precursors could be correlated to both the surface structure of the γ-Al_2O_3 support and the properties of nickel precursors. This relationship has been investigated in a series of work presented by Chen et al.[38,47,54,55] The average density of tetrahedral vacancies is higher than that of octahedral vacancies, and the dispersed Ni^{2+} ions preferentially incorporate into the tetrahedral vacancies.[38] As suggested by the incorporation model and the shielding effect of the capping anions, more tetrahedral vacancies would be shielded by larger anions. Consequently, the ratio of octahedral Ni^{2+} to tetrahedral Ni^{2+} in the sample based on the nickel precursor with larger anion would be higher than that with smaller anion.

In this work, the size of anions follows the order chloride < nitrate < acetate < acetylacetonate. Upon impregnating nickel chloride on γ-Al_2O_3, more Ni^{2+} incorporated on tetrahedral vacancies than those in the other samples due to the weak shielding effect of chloride anion. Thus, the peak area corresponding to tetrahedral site Ni^{2+} species is the largest in Ni−C. For Ni−AA, the larger acetylacetonate anions lead to the greater shielding effect, and it would be harder for Ni^{2+} to incorporate even on the octahedral sites. The 15 wt% Ni loading is relatively high. When surface sites are not enough to combine all the nickel ions, the separate NiO will be present.[41] As a result, it is the Ni−AC catalyst, not Ni−AA, that shows the largest proportion of octahedral site nickel. Excessive Ni species in Ni−AA then form bulk NiO, which can be detected in the TPR profiles (Figure 2).

Additionally, the tetrahedral site nickel corresponds to unreadily reduced nickel, and the octahedral site nickel corresponds to nickel that can be easily reduced.[41] The bulk NiO can be reduced at lower temperature (350 °C).[32] According to the distribution of Ni species on the γ-Al_2O_3, we are able to explain the different reduction degrees of the series Ni/Al_2O_3 catalysts. The lowest reduction degree in Ni−C is connected to the largest amount of unreadily reduced nickel, whereas the highest degree of Ni−AA was owed to the largest amount of bulk NiO. The reduction degree will, in turn, affect the nickel dispersion. In general, nickel dispersion could be improved with increasing the reduction degree.[36] Yet, the growth of Ni particle size with the existing excessive amount of reduced Ni is inevitable under high reduction temperature required.[56] Hence, Ni−AC and Ni−N show lower reduction degrees than Ni−AA, and their nickel particle sizes are also smaller. As for Ni−C, the largest nickel particle size is detected by both XRD and TEM. Yi et al.[33] and Hoang-Van et al.[51] also observed larger Ni particle size in the nickel chloride-derived Ni/Al_2O_3 catalyst. This could be related with the volatility of nickel chloride in the presence of hydrogen and hydrogen chloride. During the high-temperature reduction process, microscopic nickel particles produced on the support vaporize and tend to grow to large crystals.[51] In brief, anion size in the nickel precursors could have significant effect on the nickel reduction degree, dispersion, and particle size of the synthesized Ni/Al_2O_3 by distributing nickel species on different sites of γ-Al_2O_3. The Ni−AC catalyst occupies the moderate

dx.doi.org/10.1021/sc400123f | ACS Sustainable Chem. Eng. 2013, 1, 1052−1062

reduction degree, highest metal dispersion, and the smallest particle.

Consistent with the characterization results, Ni/Al_2O_3 catalysts present distinct catalytic performance in GSR. The Ni−AC catalyst shows the best performance with the highest H_2 yield under all the reaction conditions investigated. With the exception of support effect, the catalytic conversion of glycerol by steam reforming is highly affected by the nature and amount of Ni sites.[53] The Ni−AC catalyst with higher nickel dispersion could provide more active Ni sites and perform better in GSR. On the other hand, Ni−AC and Ni−N catalysts display higher CO_2/CO ratios under the same reaction parameters and hence indicate higher WGSR activity. This corresponds well with the fact that WGSR could be enhanced by smaller Ni particles.[53,57] Additionally, the nickel dispersion and particle size have significant influence on the catalytic performance of Ni/Al_2O_3 in GSR. The low Ni dispersion and large nickel particle size cause low reactivity in GSR and WGSR[58−60] and thus lead to the lowest efficiency of H_2 production. More C_2 gas-phase products in the Ni−C sample are associated with the insufficient Ni sites to cleave the C−C bond, and negligible changes of CO_2/CO ratios affirm its low WGSR activity, even under high S/C ratio.

Different degrees of deactivation are observed in 30 h stability tests. It has been widely agreed that nickel sintering and carbon deposition are two major causes of the deactivation of nickel-based catalysts at high reaction temperature.[61] However, XRD and TEM have revealed that particle size of spent catalysts does not change significantly compared with the fresh ones at the reaction condition. Even though the particle size in the Ni−C catalyst increases from 15.7 to 17.3 nm, it is not sufficient to justify the deactivation observed. Then, coke deposition forming during the steam-reforming process was investigated in an attempt to explain the deactivation phenomenon in all catalysts.

$$2CO \leftrightarrow CO_2 + C \quad \Delta H_{298\,K} = -172\ \text{kJ/mol} \tag{6}$$

Details regarding coke formation in methane and ethanol SR have been widely investigated.[62,63] The Bouduard reaction (eq 6) that is thermodynamically favored below 700 °C may lead to the coke formation. Another parallel reaction route to coking is the dehydration of the substrate to form surface olefin species, which could desorb, reformate, or polymerize to form carbonaceous deposition.[44,64,65] Indeed, the possible sources of coke formation such as ethylene, acetaldehyde, or acrolein were detected in the reaction products. Two different kinds of coke species could exist on catalysts. The mass loss below 500 °C is ascribed to filamentous or encapsulated carbonaceous deposits, and loss above 500 °C can be associated to graphitic coke with different degree of graphitization.

In Figure 10, the oxidation of Ni nanoparticles in spent catalysts leads to the slight increase of TG curves. Obvious mass loss was observed above 500 °C for all Ni/Al_2O_3 catalysts, indicating that graphite coke accounts for the main coke species. Additionally, the mass loss of Ni−C started at a bit lower temperature than the others and indicated the presence of a certain amount of filamentous carbon, which was proved in TEM images. TGA and TEM results clearly show that Ni−C catalyst contains the most serious coke deposition. The largest Ni particle Ni−C contains may be the culprit of the case, where coking and the dehydration reaction pathway are highly favored.[66−70] Additionally, the acidic property of Ni/Al_2O_3 catalysts were investigated by NH_3-TPD (Figure S2, Supporting Information), and the NH_3 desorption curves reveal that Ni−C is rich in both medium−strong and strong acidic sites.[8,71] Acid sites could promote the reactions of dehydration and aldol condensation, which therefore cause serious carbon deposition.[53] Yet, relatively good and stable performance can be observed on the Ni−AC catalyst (Figure 8), together with the lowest carbon deposition. This indicates that smaller nickel particle sizes and higher dispersion achieved over the Ni−AC would be less prone to coking due to the larger interface between the active metal and the support. The amount of coke deposition follows the order Ni−AC < Ni−N < Ni−AA < Ni−C. Specifically, this order matches not just with that of the nickel particle sizes but also with the performance in the stability test. Hence, it could be concluded that coke deposition—mainly graphite species—leads to the deactivation of catalysts in GSR, and the amount of coke is highly related to the nickel particle sizes and dispersion of Ni/Al_2O_3 catalysts based on different nickel precursors.

CONCLUSIONS

The present work highlights the importance of anion size of the nickel precursor, which plays a key role in distributing Ni^{2+} on the tetrahedral and octahedral vacancies of γ-Al_2O_3. Upon calcination and reduction, Ni/Al_2O_3 catalysts based on different precursors could present distinct characteristics in nickel dispersion, reduction degree, and particle size. These characteristics prove to have profound influence on the GSR activity. Ni−AC, with high nickel dispersion, small particle size, and moderate reduction degree, has the highest H_2 yield and best reaction stability. Additionally, the optimized reaction parameters for GSR are 550 °C and S/C = 3 in terms of the efficiency of H_2 production and energy consumption. Coke deposition, not nickel sintering, is deemed to cause the deactivation of catalysts in GSR, and the graphite species primarily accounts for the coke formation. Nickel particle size and dispersion are found to be related with the amount of coke deposition. Serious coke deposition and low GSR activity of Ni−C could be ascribed to the large Ni particle size, low Ni dispersion, and residual chloride.

ASSOCIATED CONTENT

Supporting Information

Figures giving XPS spectra of Ni−C and NH_3-TPD profiles of Ni/Al_2O_3 catalysts. This material is available free of charge via the Internet at http://pubs.acs.org.

AUTHOR INFORMATION

Corresponding Author

*E-mail: jlgong@tju.edu.cn. Fax: (+86) 22-87401818.

Notes

The authors declare no competing financial interest.

ACKNOWLEDGMENTS

We thank the Natural Science Foundation of China (21006068, 21222604, 21206115), Program for New Century Excellent Talents in University (NCET-10-0611), Specialized Research Fund for the Doctoral Program of Higher Education (20120032110024), Scientific Research Foundation for the Returned Overseas Chinese Scholars (MoE), Seed Foundation of Tianjin University (60303002), and Program of Introducing Talents of Discipline to Universities (B06006) for funding.

REFERENCES

(1) Ochoa-Fernandez, E.; Haugen, G.; Zhao, T.; Ronning, M.; Aartun, I.; Borresen, B.; Rytter, E.; Ronnekleiv, M.; Chen, D. Process design simulation of H_2 production by sorption enhanced steam methane reforming: Evaluation of potential CO_2 acceptors. *Green Chem.* **2007**, *9* (6), 654−662.

(2) Pirez, C.; Capron, M.; Jobic, H.; Dumeignil, F.; Jalowiecki-Duhamel, L. Highly efficient and stable $CeNiH_ZO_Y$ nano-oxyhydride catalyst for H_2 production from ethanol at room temperature. *Angew. Chem., Int. Ed.* **2011**, *50* (43), 10193−10197.

(3) Chen, D.; He, L. Towards an efficient hydrogen production from biomass: A review of processes and materials. *ChemCatChem* **2011**, *3* (3), 490−511.

(4) He, L.; Parra, J. M. S.; Blekkan, E. A.; Chen, D. Towards efficient hydrogen production from glycerol by sorption enhanced steam reforming. *Energ. Environ. Sci.* **2010**, *3* (8), 1046−1056.

(5) Gallo, A.; Pirovano, C.; Ferrini, P.; Marelli, M.; Psaro, R.; Santangelo, S.; Faggio, G.; Dal Santo, V. Influence of reaction parameters on the activity of ruthenium based catalysts for glycerol steam reforming. *Appl. Catal., B* **2012**, *121−122* (0), 40−49.

(6) Piscina, P. R. d. l.; Homs, N. Use of biofuels to produce hydrogen (reformation processes). *Chem. Soc. Rev.* **2008**, *37* (11), 2459−2467.

(7) Alonso, D. M.; Wettstein, S. G.; Dumesic, J. A. Bimetallic catalysts for upgrading of biomass to fuels and chemicals. *Chem. Soc. Rev.* **2012**, *41*, 8075−8098.

(8) Li, S.; Zhang, C.; Zhang, P.; Wu, G.; Ma, X.; Gong, J. On the origin of reactivity of steam reforming of ethylene glycol on supported Ni catalysts. *Phys. Chem. Chem. Phys.* **2012**, *14* (12), 4066−4069.

(9) Zhang, C.; Yue, H.; Huang, Z.; Li, S.; Wu, G.; Ma, X.; Gong, J. Hydrogen production via steam reforming of ethanol on phyllosilicate-derived Ni/SiO_2: Enhanced metal−support interaction and catalytic stability. *ACS Sustainable Chem. Eng.* **2012**, *1* (1), 161−173.

(10) Cui, Y.; Galvita, V.; Rihko-Struckmann, L.; Lorenz, H.; Sundmacher, K. Steam reforming of glycerol: The experimental activity of $La_{1-x}Ce_xNiO_3$ catalyst in comparison to the thermodynamic reaction equilibrium. *Appl. Catal., B* **2009**, *90* (1−2), 29−37.

(11) Bobadilla, L. F.; Álvarez, A.; Domínguez, M. I.; Romero-Sarria, F.; Centeno, M. A.; Montes, M.; Odriozola, J. A. Influence of the shape of Ni catalysts in the glycerol steam reforming. *Appl. Catal., B* **2012**, *123−124* (0), 379−390.

(12) Soares, R. R.; Simonetti, D. A.; Dumesic, J. A. Glycerol as a source for fuels and chemicals by low-temperature catalytic processing. *Angew. Chem., Int. Ed. Engl.* **2006**, *45* (24), 3982−5.

(13) Pagliaro, M.; Ciriminna, R.; Kimura, H.; Rossi, M.; Della Pina, C. From glycerol to value-added products. *Angew. Chem., Int. Ed.* **2007**, *46* (24), 4434−4440.

(14) Zhou, C. H.; Beltramini, J. N.; Fan, Y. X.; Lu, G. Q. Chemoselective catalytic conversion of glycerol as a biorenewable source to valuable commodity chemicals. *Chem. Soc. Rev.* **2008**, *37* (3), 527−49.

(15) Pompeo, F.; Santori, G.; Nichio, N. N. Hydrogen and/or syngas from steam reforming of glycerol. Study of platinum catalysts. *Int. J. Hydrogen Energy* **2010**, *35* (17), 8912−8920.

(16) Zhang, C.; Zhang, P.; Li, S.; Wu, G.; Ma, X.; Gong, J. Superior reactivity of skeletal Ni-based catalysts for low-temperature steam reforming to produce CO-free hydrogen. *Phys. Chem. Chem. Phys.* **2012**, *14* (10), 3295−3298.

(17) Chiodo, V.; Freni, S.; Galvagno, A.; Mondello, N.; Frusteri, F. Catalytic features of Rh and Ni supported catalysts in the steam reforming of glycerol to produce hydrogen. *Appl. Catal., A* **2010**, *381* (1−2), 1−7.

(18) Nichele, V.; Signoretto, M.; Menegazzo, F.; Gallo, A.; Dal Santo, V.; Cruciani, G.; Cerrato, G. Glycerol steam reforming for hydrogen production: Design of Ni supported catalysts. *Appl. Catal., B* **2012**, *111−112* (0), 225−232.

(19) Kunkes, E. L.; Soares, R. R.; Simonetti, D. A.; Dumesic, J. A. An integrated catalytic approach for the production of hydrogen by glycerol reforming coupled with water-gas shift. *Appl. Catal., B.* **2009**, *90* (3−4), 693−698.

(20) Byrd, A.; Pant, K.; Gupta, R. Hydrogen production from glycerol by reforming in supercritical water over Ru/Al_2O_3 catalyst. *Fuel* **2008**, *87* (13−14), 2956−2960.

(21) Zhang, B.; Tang, X.; Li, Y.; Xu, Y.; Shen, W. Hydrogen production from steam reforming of ethanol and glycerol over ceria-supported metal catalysts. *Int. J. Hydrogen Energy* **2007**, *32* (13), 2367−2373.

(22) Vaidya, P. D.; Rodrigues, A. E. Glycerol reforming for hydrogen production: A review. *Chem. Eng. Technol.* **2009**, *32* (10), 1463−1469.

(23) Adhikari, S.; Fernando, S. D.; Haryanto, A. Hydrogen production from glycerol: An update. *Energy Convers. Manage.* **2009**, *50* (10), 2600−2604.

(24) Dal Santo, V.; Gallo, A.; Naldoni, A.; Guidotti, M.; Psaro, R. Bimetallic heterogeneous catalysts for hydrogen production. *Catal. Today* **2012**, *197* (1), 190−205.

(25) Adhikari, S.; Fernando, S.; Haryanto, A. A Comparative Thermodynamic and experimental analysis on hydrogen production by steam reforming of glycerin. *Energy Fuels* **2007**, *21* (4), 2306−2310.

(26) Adhikari, S.; Fernando, S.; Haryanto, A. Production of hydrogen by steam reforming of glycerin over alumina-supported metal catalysts. *Catal. Today* **2007**, *129* (3−4), 355−364.

(27) Cui, Y.; Galvita, V.; Rihko-Struckmann, L.; Lorenz, H.; Sundmacher, K. Steam reforming of glycerol: The experimental activity of $La_{1-x}Ce_xNiO_3$ catalyst in comparison to the thermodynamic reaction equilibrium. *Appl. Catal., B* **2009**, *90* (1−2), 29−37.

(28) Davda, R. R.; Shabaker, J. W.; Huber, G. W.; Cortright, R. D.; Dumesic, J. A. A review of catalytic issues and process conditions for renewable hydrogen and alkanes by aqueous-phase reforming of oxygenated hydrocarbons over supported metal catalysts. *Appl. Catal., B* **2005**, *56* (1−2), 171−186.

(29) Rossetti, I.; Gallo, A.; Dal Santo, V.; Bianchi, C. L.; Nichele, V.; Signoretto, M.; Finocchio, E.; Ramis, G.; Di Michele, A. Nickel catalysts supported over TiO_2, SiO_2 and ZrO_2 for the steam reforming of glycerol. *ChemCatChem* **2013**, *5* (1), 294−306.

(30) Li, S.; Li, M.; Zhang, C.; Wang, S.; Ma, X.; Gong, J. Steam reforming of ethanol over Ni/ZrO2 catalysts: Effect of support on product distribution. *Int. J. Hydrogen Energy* **2012**, *37* (3), 2940−2949.

(31) Zhang, C.; Li, S.; Li, M.; Wang, S.; Ma, X.; Gong, J. Enhanced oxygen mobility and reactivity for ethanol steam reforming. *AIChE J.* **2012**, *58* (2), 516−525.

(32) Ruckenstein, E.; Hu, Y. H. Interactions between Ni and La_2O_3in Ni/La_2O_3 catalysts prepared using different Ni precursors. *J. Catal.* **1996**, *161* (1), 55−61.

(33) Kim, P.; Kim, H.; Joo, J. B.; Kim, W.; Song, I. K.; Yi, J. Effect of nickel precursor on the catalytic performance of Ni/Al_2O_3 catalysts in the hydrodechlorination of 1,1,2-trichloroethane. *J. Mol. Catal. A: Chem.* **2006**, *256* (1−2), 178−183.

(34) Fang, K.; Ren, J.; Sun, Y. Effect of nickel precursors on the performance of Ni/AlMCM-41 catalysts for n-dodecane hydroconversion. *J. Mol. Catal. A: Chem.* **2005**, *229* (1−2), 51−58.

(35) Álvarez-Rodríguez, J.; Cerro-Alarcón, M.; Guerrero-Ruiz, A.; Rodríguez-Ramos, I.; Arcoya, A. Effect of nickel precursor and the copper addition on the surface properties of Ni/KL-supported catalysts for selective hydrogenation of citral. *Appl. Catal., A* **2008**, *348* (2), 241−250.

(36) Wang, S.; Lu, G. Q. Reforming of methane with carbon dioxide over Ni/Al_2O_3 catalysts: Effect of nickel precursor. *Appl. Catal., A* **1998**, *169* (2), 271−280.

(37) Li, F.; Yi, X.; Fang, W. Effect of organic nickel precursor on the reduction performance and hydrogenation activity of Ni/Al_2O_3 catalysts. *Catal. Lett.* **2009**, *130* (3), 335−340.

(38) Ren, S.; Qiu, J.; Wang, C.; Xu, B.; Fan, Y.; Chen, Y. Influence of nickel salt precursors on the hydrogenation activity of $Ni/\gamma\text{-}Al_2O_3$ Catalyst. *Chin. J. Catal.* **2007**, *28* (7), 651−656.

(39) Tsoncheva, T.; Vankova, S.; Mehandjiev, D. Effect of the precursor and the preparation method on copper based activated carbon catalysts for methanol decomposition to hydrogen and carbon monoxide. *Fuel* **2003**, *82* (7), 755−763.

(40) Topsøe, H.; Clausen, B. S. Active sites and support effects in hydrodesulfurization catalysts. *Appl. Catal.* **1986**, *25* (1−2), 273−293.
(41) Wu, M.; Hercules, D. M. Studies of supported nickel catalysts by X-ray photoelectron and ion scattering spectroscopies. *J. Phys. Chem.* **1979**, *83* (15), 2003−2008.
(42) Wang, X.; Zhao, B.; Jiang, D.-e.; Xie, Y. Monolayer dispersion of MoO_3, NiO and their precursors on γ-Al_2O_3. *Appl. Catal., A* **1999**, *188* (1−2), 201−209.
(43) Wang, X.; Li, S.; Wang, H.; Liu, B.; Ma, X. Thermodynamic analysis of glycerin steam reforming. *Energy Fuels* **2008**, *22* (6), 4285−4291.
(44) Iriondo, A.; Cambra, J. F.; Güemez, M. B.; Barrio, V. L.; Requies, J.; Sánchez-Sánchez, M. C.; Navarro, R. M. Effect of ZrO_2 addition on Ni/Al_2O_3 catalyst to produce H_2 from glycerol. *Int. J. Hydrogen Energy* **2012**, *37* (8), 7084−7093.
(45) Chen, J.; Wang, R.; Zhang, J.; He, F.; Han, S. Effects of preparation methods on properties of Ni/CeO_2−Al_2O_3 catalysts for methane reforming with carbon dioxide. *J. Mol. Catal. A: Chem.* **2005**, *235* (1−2), 302−310.
(46) Li, G.; Hu, L.; Hill, J. M. Comparison of reducibility and stability of alumina-supported Ni catalysts prepared by impregnation and co-precipitation. *Appl. Catal., A* **2006**, *301* (1), 16−24.
(47) Zhang, L.; Lin, J.; Chen, Y. Characterization of dispersion and surface states of NiO/γ-alumina and NiO/La_2O_3-γ-alumina catalysts. *J. Chem. Soc., Faraday Trans.* **1992**, *88* (3), 497−502.
(48) Schuit, G. C. A.; Gates, B. C. Chemistry and engineering of catalytic hydrodesulfurization. *AIChE J.* **1973**, *19* (3), 417−438.
(49) Wu, G.; Zhang, C.; Li, S.; Huang, Z.; Yan, S.; Wang, S.; Ma, X.; Gong, J. Sorption enhanced steam reforming of ethanol on Ni−CaO−Al_2O_3 multifunctional catalysts derived from hydrotalcite-like compounds. *Energy Environ. Sci.* **2012**, *5* (10), 8942.
(50) Sánchez, E. A.; D'Angelo, M. A.; Comelli, R. A. Hydrogen production from glycerol on Ni/Al_2O_3 catalyst. *Int. J. Hydrogen Energy* **2010**, *35* (11), 5902−5907.
(51) Hoang-Van, C.; Kachaya, Y.; Teichner, S. J.; Arnaud, Y.; Dalmon, J. A. Characterization of nickel catalysts by chemisorption techniques, X-ray diffraction and magnetic measurements: Effects of support, precursor and hydrogen pretreatment. *Appl. Catal.* **1989**, *46* (2), 281−296.
(52) Araque, M.; Martínez T, L. M.; Vargas, J. C.; Centeno, M. A.; Roger, A. C. Effect of the active metals on the selective H_2 production in glycerol steam reforming. *Appl. Catal., B* **2012**, *125* (0), 556−566.
(53) Kim, S. M.; Woo, S. I. Sustainable production of syngas from biomass-derived glycerol by steam reforming over highly stable Ni/SiC. *ChemSusChem* **2012**, *5* (8), 1513−1522.
(54) Chen, Y.; Zhang, L. Surface interaction model of γ-alumina-supported metal oxides. *Catal. Lett.* **1992**, *12* (1), 51−62.
(55) Lin Dong, Y. C. Study on the interaction between ionic compounds and oxide supports —"Incorporation model" and its application. *Chin. J. Inorg. Chem.* **2000**, *16* (2), 250−260.
(56) Bolt, P. H.; Habraken, F. H. P. M.; Geus, J. W. On the role of a $NiAl_2O_4$ intermediate layer in the sintering behavior of Ni/α−Al_2O_3. *J. Catal.* **1995**, *151* (2), 300−306.
(57) Li, Y.; Fu, Q.; Flytzani-Stephanopoulos, M. Low-temperature water-gas shift reaction over Cu- and Ni-loaded cerium oxide catalysts. *Appl. Catal., B* **2000**, *27* (3), 179−191.
(58) Adhikari, S.; Fernando, S. D.; To, S. D. F.; Bricka, R. M.; Steele, P. H.; Haryanto, A. Conversion of glycerol to hydrogen via a steam reforming process over nickel catalysts. *Energy Fuels* **2008**, *22* (2), 1220−1226.
(59) Iriondo, A.; Barrio, V. L.; Cambra, J. F.; Arias, P. L.; Güemez, M. B.; Navarro, R. M.; Sanchez-Sanchez, M. C.; Fierro, J. L. G. Influence of La_2O_3 modified support and Ni and Pt active phases on glycerol steam reforming to produce hydrogen. *Catal. Commun.* **2009**, *10* (8), 1275−1278.
(60) Buffoni, I. N.; Pompeo, F.; Santori, G. F.; Nichio, N. N. Nickel catalysts applied in steam reforming of glycerol for hydrogen production. *Catal. Commun.* **2009**, *10* (13), 1656−1660.
(61) Li, S.; Zhang, C.; Huang, Z.; Wu, G.; Gong, J. A Ni@ZrO_2 nanocomposite for ethanol steam reforming: enhanced stability via strong metal-oxide interaction. *Chem. Commun.* **2013**, *49* (39), 4226−4228.
(62) Benito, M.; Padilla, R.; Serrano-Lotina, A.; Rodríguez, L.; Brey, J. J.; Daza, L. The role of surface reactions on the active and selective catalyst design for bioethanol steam reforming. *J. Power Sources* **2009**, *192* (1), 158−164.
(63) Wang, F.; Li, Y.; Cai, W.; Zhan, E.; Mu, X.; Shen, W. Ethanol steam reforming over Ni and Ni−Cu catalysts. *Catal. Today* **2009**, *146* (1−2), 31−36.
(64) Iriondo, A.; Barrio, V. L.; Cambra, J. F.; Arias, P. L.; Guemez, M. B.; Sanchez-Sanchez, M. C.; Navarro, R. M.; Fierro, J. L. G. Glycerol steam reforming over Ni catalysts supported on ceria and ceria-promoted alumina. *Int. J. Hydrogen Energy* **2010**, *35* (20), 11622−11633.
(65) Iriondo, A.; Cambra, J. F.; Barrio, V. L.; Guemez, M. B.; Arias, P. L.; Sanchez-Sanchez, M. C.; Navarro, R. M.; Fierro, J. L. G. Glycerol liquid phase conversion over monometallic and bimetallic catalysts: Effect of metal, support type and reaction temperatures. *Appl. Catal., B* **2011**, *106* (1−2), 83−93.
(66) Vizcaíno, A. J.; Carrero, A.; Calles, J. A. Ethanol steam reforming on Mg- and Ca-modified Cu−Ni/SBA-15 catalysts. *Catal. Today* **2009**, *146* (1−2), 63−70.
(67) Christensen, K. O.; Chen, D.; Lødeng, R.; Holmen, A. Effect of supports and Ni crystal size on carbon formation and sintering during steam methane reforming. *Appl. Catal., A* **2006**, *314* (1), 9−22.
(68) Centi, G.; Perathoner, S. Opportunities and prospects in the chemical recycling of carbon dioxide to fuels. *Catal. Today* **2009**, *148* (3−4), 191−205.
(69) Chen, D.; Christensen, K. O.; Ochoa-Fernández, E.; Yu, Z.; Tøtdal, B.; Latorre, N.; Monzón, A.; Holmen, A. Synthesis of carbon nanofibers: Effects of Ni crystal size during methane decomposition. *J. Catal.* **2005**, *229* (1), 82−96.
(70) Gonzalez-DelaCruz, V. M.; Holgado, J. P.; Pereñíguez, R.; Caballero, A. Morphology changes induced by strong metal−support interaction on a Ni−ceria catalytic system. *J. Catal.* **2008**, *257* (2), 307−314.
(71) Galetti, A. E.; Gomez, M. F.; Arrúa, L. A.; Abello, M. C. Hydrogen production by ethanol reforming over NiZnAl catalysts. *Appl. Catal., A* **2008**, *348* (1), 94−102.